Virus-induced hepatocellular carcinomas cause antigen-specific local tolerance

Gerald Willimsky,[1,2] Karin Schmidt,[1] Christoph Loddenkemper,[3] Johanna Gellermann,[4] and Thomas Blankenstein[1,2]

[1]Institute of Immunology, Charité Campus Benjamin Franklin, Berlin, Germany. [2]Max Delbrück Center for Molecular Medicine, Berlin, Germany. [3]Institute of Pathology, Charité Campus Benjamin Franklin, Berlin, Germany. [4]Clinic for Radiation Medicine, Charité Campus Berlin Buch, Berlin, Germany.

T cell surveillance is often effective against virus-associated tumors because of their high immunogenicity. It is not clear why surveillance occasionally fails, particularly against hepatitis B virus– or hepatitis C virus–associated hepatocellular carcinoma (HCC). We established a transgenic murine model of virus-induced HCC by hepatocyte-specific adenovirus-induced activation of the oncogenic SV40 large T antigen (TAg). Adenovirus infection induced cytotoxic T lymphocytes (CTLs) targeted against the virus and TAg, leading to clearance of the infected cells. Despite the presence of functional, antigen-specific T cells, a few virus-infected cells escaped immune clearance and progressed to HCC. These cells expressed TAg at levels similar to HCC isolated from neonatal TAg-tolerant mice, suggesting that CTL clearance does not select for cells with low immunogenicity. Virus-infected mice revealed significantly greater T cell infiltration in early-stage HCC compared with that in late-stage HCC, demonstrating progressive local immune suppression through inefficient T cell infiltration. Programmed cell death protein-1 (PD-1) and its ligand PD-L1 were expressed in all TAg-specific CD8$^+$ T cells and HCC, respectively, which contributed to local tumor-antigen-specific tolerance. Thus, we have developed a model of virus-induced HCC that may allow for a better understanding of human HCC.

Introduction

T cell surveillance is often effective against virus-induced tumors because of their high immunogenicity (1, 2). It remains unclear why surveillance occasionally fails, e.g., against hepatitis B virus–associated (HBV-associated) or hepatitis C virus–associated (HCV-associated) hepatocellular carcinoma (HCC). Possible reasons could be an initial failure to induce effective T cells (3–5), T cell exhaustion due to chronic antigen stimulation (6, 7), tumor-induced tolerance (8), immune escape by loss of immunogenicity (9), or tumor development in tolerogenic organs, e.g., the liver (10). In humans, T cell responses appear to be more efficient in those individuals who completely cleared the virus (11, 12); however, it is difficult to identify individuals in the acute infection phase (4, 12). HCC progresses in a great proportion of individuals with chronic HCV infection in the presence of virus-specific CD8$^+$ T cells (13–15). On the other hand, impaired HCV-specific T cell responses have been observed in PBMCs or liver biopsies obtained from patients with chronic HCV infection (4, 16–18). Heterogeneity within individuals, difficulties in analyzing local T cell responses, and the need of in vitro manipulation and expansion for functional analysis of HCV-specific T cells make firm conclusions difficult. Likewise, in chimpanzees, no strict correlation between virus clearance and vigorous T cell responses was observed (19, 20).

Several HCV transgenic mouse lines with constitutive or inducible HCV expression and models that allow infection of hepatocytes by HCV have been generated (21–28). While these models have yielded important information about viral pathogenesis, the mice were either tolerant for viral antigens or did not develop HCC with reliable, high frequency. Thus, the endogenous T cell response to virus-induced HCC throughout the course of the disease has not been analyzed. To overcome the problem of T cell tolerance to viral antigens, T cells from HBV-immunized wild-type mice were transferred into HBV transgenic mice. The data showed that CD8$^+$ T cells were mainly responsible for hepatitis and that viral replication was abolished by cytolytic and noncytolytic mechanisms (29). The chronic necroinflammatory T cell response was suggested to contribute to HCC development (30). On the other hand, HCC developed in some HCV transgenic mice independent of inflammation (25), and it is not clear whether the fate of adoptively transferred CD8$^+$ T cells recapitulates that of the endogenous T cell pool following viral infection. Here, we established a model of virus-induced HCC, in which a viral oncogene, SV40 large T antigen (TAg), was activated in hepatocytes through viral infection of a host, LoxP-TAg mice, that can efficiently respond to TAg. In LoxP-TAg mice, Cre recombinase–encoding adenoviruses (Ad.Cre) with high tropism for the liver deleted a stop cassette, which prevented TAg expression. Previously, we have shown that these mice have retained CD8$^+$ T cells against peptide IV (pIV), the dominant epitope of TAg, which could be induced by prophylactic immunization for protection from sporadic tumors that occur late in life (8, 31). In contrast to mice with virus-induced HCC reported here, mice with sporadic lesions readily developed TAg-specific CD8$^+$ T cell tolerance.

Results

Virus-induced oncogene activation and HCC development. LoxP-TAg mice allow activation of the dormant TAg oncogene by Cre/loxP recombinase–mediated stop cassette deletion (Figure 1A). Based on Ad.Cre infection of the liver we established a model for virus-induced HCC. LoxP-TAg mice were injected i.v. with Ad.Cre and monitored for tumor development by MRI, palpation, and determination of liver enzymes alanine aminotransferase (ALT) and aspartate transaminase (AST). By MRI, tumors of around 2.5 × 2.5 mm in size were

Authorship note: Gerald Willimsky and Karin Schmidt contributed equally to this work.

Conflict of interest: The authors have declared that no conflict of interest exists.

Citation for this article: *J Clin Invest.* 2013;123(3):1032–1043. doi:10.1172/JCI64742.

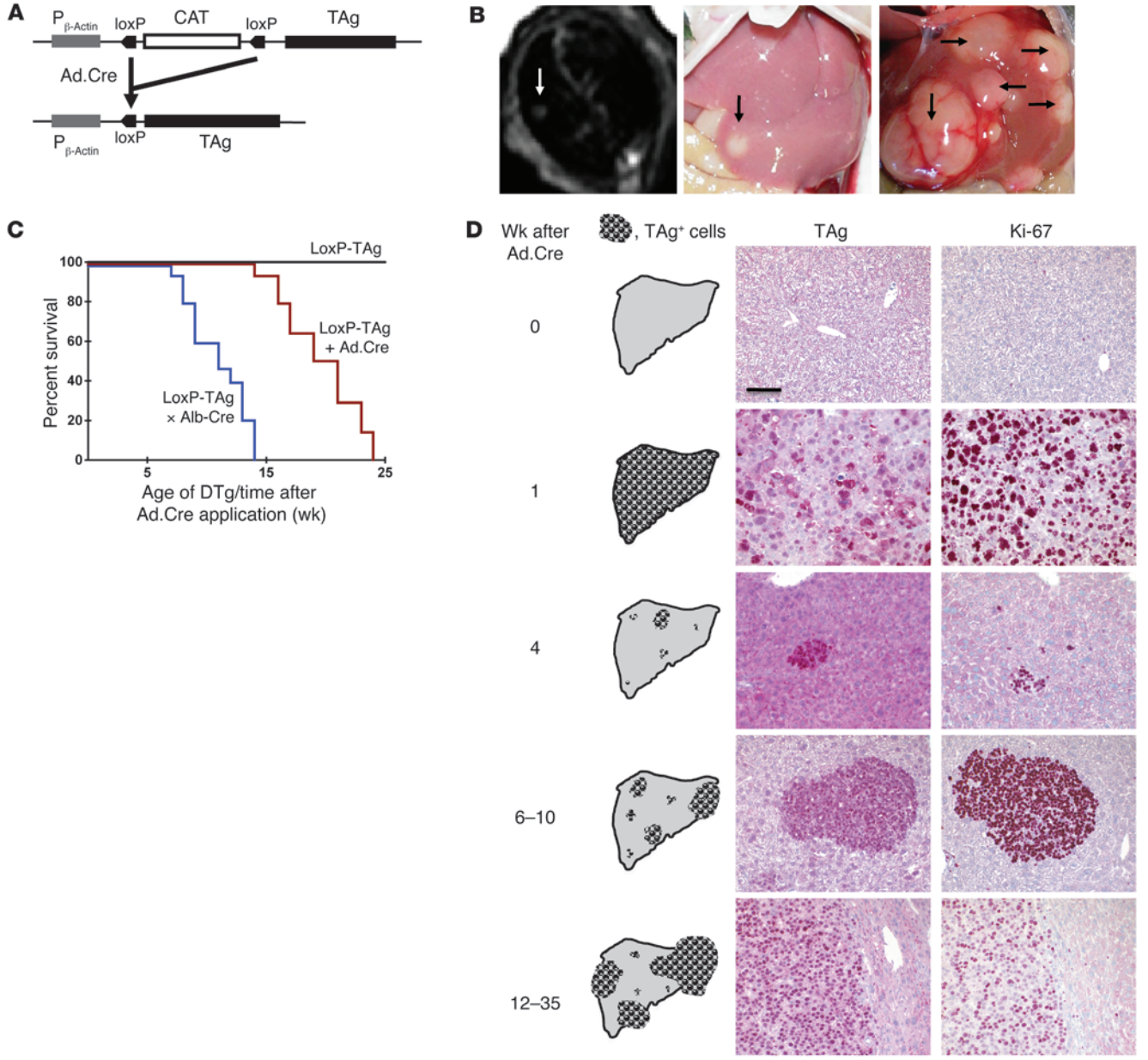

Figure 1

LoxP-TAg transgenic mice develop HCC after i.v. injection of Ad.Cre. (**A**) Cre recombinase–mediated TAg activation. (**B**) For induction of HCC, 8- to 12-week-old LoxP-TAg mice were injected i.v. with 1×10^9 PFUs of Ad.Cre, and HCC development was detected by MRI and palpation. Representative MR images (left) and macroscopically visible tumors of livers 10 (middle) and 20 weeks (right) after Ad.Cre injection are shown. MR image and liver photograph (middle) are from the same mouse. Arrows indicate tumor nodules. (**C**) LoxP-TAg mice that received Ad.Cre (red line, $n = 14$) and double-transgenic LoxP-TAg × Alb-Cre (DTg) mice (blue line, $n = 15$) were monitored for HCC development. Nontreated LoxP-TAg mice (black line; $n = 10$) served as control. Time after adenovirus injection is given for Ad.Cre-injected mice, and age is given for double-transgenic LoxP-TAg × Alb-Cre mice. (**D**) Immunohistology of liver tissue sections of LoxP-TAg mice at different time points after Ad.Cre injection as indicated. Tissues were stained with antibodies specific for TAg and Ki-67 and counterstained with hematoxylin. Scale bar: 100 μm. At least 3 mice were analyzed for each time point, and a representative staining is shown. Schematic drawings show an overview of the cumulative data of the average tumor number and progression not considering inter-mouse variability.

detected in the liver 8–16 weeks after virus infection (Figure 1B). Elevated ALT and AST levels were detected 1 week after virus infection, indicating liver damage (Supplemental Figure 1; supplemental material available online with this article; doi:10.1172/JCI64742DS1). After 4 to 6 weeks, ALT/AST values returned to slightly elevated levels, when compared with those of control mice, and subsequently increased proportionally to HCC development. The virus-induced TAg activation induced multinodular HCC of classical type, resembling hepatocytes with a predominantly trabecular (plate-like) architectural pattern within 8 to 24 weeks (in some

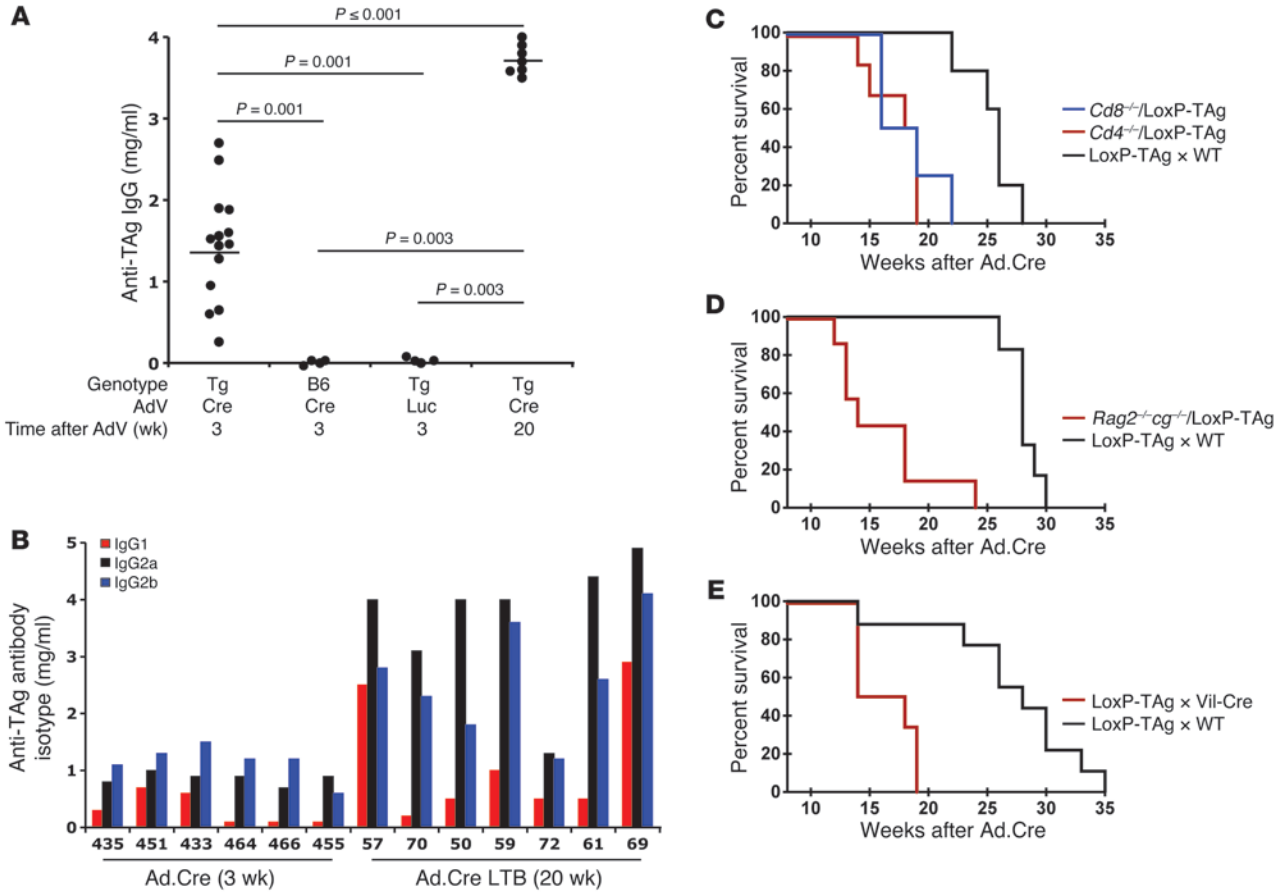

Figure 2

Immunity to the cancer-driving oncogene following virus-induced activation. (**A**) The amount of TAg-specific IgG antibodies was determined in serum obtained from B6 (n = 4) and LoxP-TAg mice (Tg) 3 (n = 14) and 20 weeks (n = 7) after i.v. injection of Ad.Cre (1 × 10^9 PFUs). Bars indicate mean values. As controls, LoxP-TAg mice were i.v. injected with 1 × 10^9 PFUs of Ad.Luc (n = 4). LoxP-TAg mice analyzed 20 weeks after Ad.Cre injection had macroscopically visible tumors (see Figure 1, B and D). (**B**) LoxP-TAg mice develop TAg-specific antibodies of IgG1, IgG2a, and IgG2b isotypes upon Ad.Cre-mediated TAg activation. Amounts of TAg-specific IgG1, IgG2a, IgG2b, and IgG3 were determined in serum obtained from individual mice 3 and 20 weeks after Ad.Cre application. IgG3 was not detectable in any serum sample (not shown). Each number represents an individual mouse. LTB, large tumor bearing. (**C**) $CD4^+$ T cell–deficient ($Cd4^{-/-}$ × LoxP-TAg; n = 6) and $CD8^+$ T cell–deficient mice ($Cd8^{-/-}$ × LoxP-TAg; n = 4) received 1 × 10^9 PFUs of Ad.Cre and were monitored for HCC development. Ad.Cre-treated T cell–competent LoxP-TAg mice (WT × LoxP-TAg; n = 5) served as controls. (**D**) Ad.Cre-treated $Rag2^{-/-}cg^{-/-}$ × LoxP-TAg mice (n = 7) were monitored for HCC development. LoxP-TAg mice (n = 6) served as control. (**E**) TAg-tolerant Vil-Cre × LoxP-TAg mice (n = 6) were injected with 1 × 10^9 PFUs of Ad.Cre and monitored for HCC development. LoxP-TAg mice (n = 9) served as controls. (**C**–**E**) Time after adenovirus infection is given.

mice 35 weeks) (Figure 1, C and D, and Supplemental Figure 2). In comparison, neonatal TAg-tolerant LoxP-TAg × albumin-Cre (Alb-Cre) mice that express the Cre recombinase by the albumin promoter and activate TAg in the liver early in life developed HCC within 7 to 14 weeks of age (Figure 1C). Upon liver tumor development, LoxP-TAg × Alb-Cre mice showed an increase of ALT/AST values that stayed elevated until mice succumbed to HCC and cholangiolar carcinoma (Supplemental Figure 3). Nontreated LoxP-TAg mice did not develop HCC or pathological abnormalities in the liver during the more than 12-month observation time, as assessed by MRI, histology (data not shown), and determination of liver enzymes ALT and AST (Supplemental Figure 4). TAg expression was abundantly detected throughout the liver 1 week after viral infection (Figure 1D). Ki-67 expression often mirrored TAg expression, indicating abundant cell proliferation in TAg-expressing hepatocytes. Within the next 3 weeks, TAg^+ cells were almost completely eliminated, leaving behind few microscopically small TAg^+ lesions, which then progressed to HCC (Figure 1D).

TAg recognition during viral infection induces T cell immunity. Our model is based on the assumption that the stop cassette is deleted and TAg is activated in virus-infected liver cells and that TAg is recognized by the adaptive immune system concomitant with a strong antiadenoviral immune response. Within 3 weeks after Ad.Cre infection, LoxP-TAg mice developed high anti-TAg IgG antibody titers, demonstrating that TAg was rapidly recognized by the adaptive immune system and suggesting functional $CD4^+$ T cell activation (Figure 2A). Neither Ad.Cre infection of C57BL/6 (B6) mice nor luciferase-encoding adenovirus (Ad.Luc) infection of LoxP-TAg mice induced anti-TAg antibodies. Bioluminescence (BL) imaging of Ad.Luc-infected LoxP-TAg mice confirmed the high tropism for the liver (Supplemental Figure 5). The TAg-specific IgG antibodies were of IgG1, IgG2a, and IgG2b isotypes (Figure 2B). Because

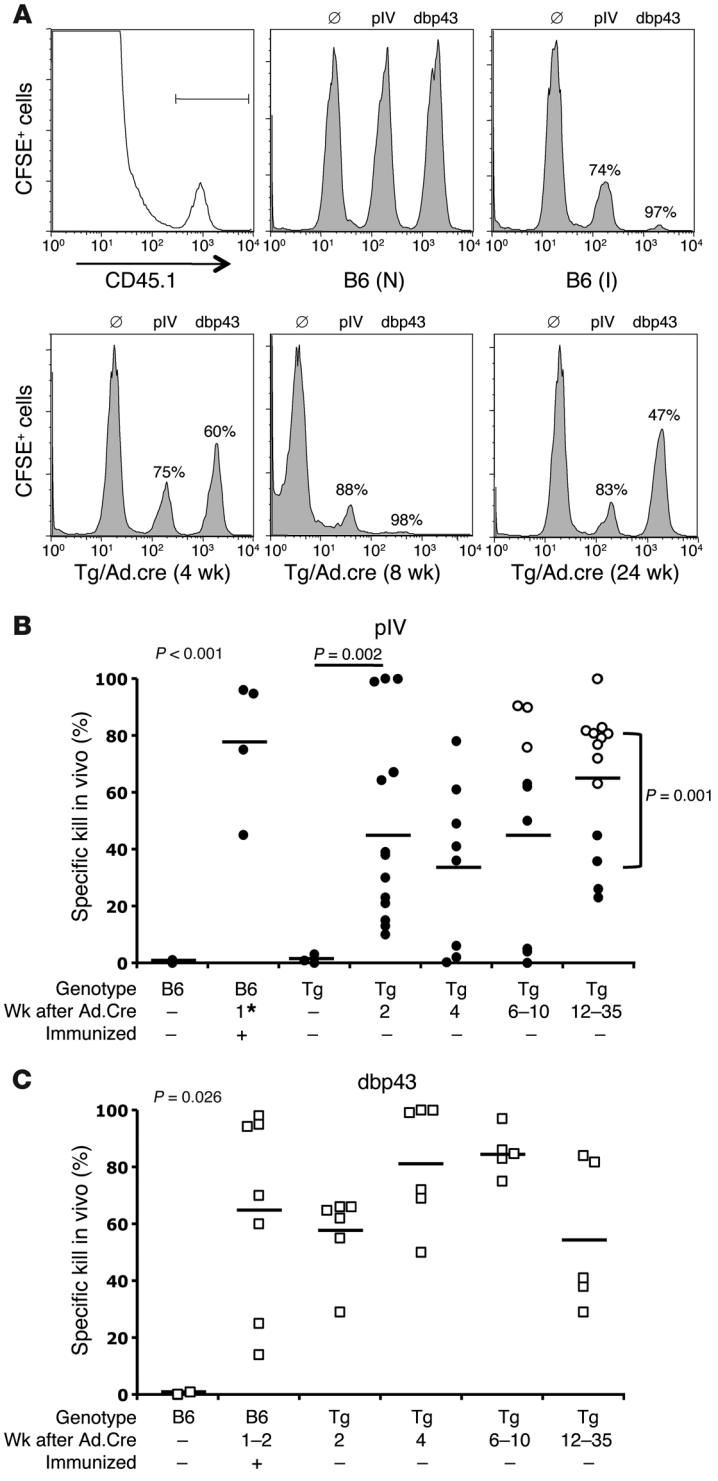

Figure 3

Ad.Cre-mediated TAg activation in LoxP-TAg mice induces functional pIV-specific CTLs, which increase with tumor burden. CTL activity against pIV alone or simultaneously against pIV and adenovirus dbp43 was analyzed in vivo. For simultaneous detection of CTL activity against pIV and dbp43, nonloaded and pIV- and dbp43-loaded CD45.1 congenic spleen cells (1×10^7 each) were labeled with different amounts of CFSE and injected into the indicated mice, and 18 hours later the ratio between different populations was determined by flow cytometry, gated on CD45.1$^+$ cells. The percentage of specific killing is indicated. In some experiments, only pIV-specific CTLs were analyzed. (**A**) Gating for the injected CD45.1$^+$ spleen cells and one representative example per experimental group is shown for the simultaneous detection of pIV and dbp43 CTLs. Naive 8- to 12-week-old B6 (N), immunized 8- to 12-week-old B6 (I), and 8- to 12-week-old LoxP-TAg (Tg) mice 2, 4, 6–10, and 12–35 weeks after Ad.Cre injection were analyzed. Immunization of B6 mice was performed either by single i.p. injection of 0.5×10^7 to 1×10^7 16.113 cells or simultaneous injection of 16.113 cells (i.p.) and 1×10^9 PFUs Ad.Cre (i.v.). (**B**) The combined data of pIV-specific kill are shown. White circles represent LoxP-TAg mice with liver tumors larger than 5 mm in diameter. Black circles represent B6 and LoxP-TAg mice with no tumors or LoxP-TAg mice with liver tumors smaller than 5 mm in diameter. Each symbol represents 1 mouse; horizontal bars indicate mean values. Some of the B6 mice were injected with 16.113 only (asterisk). The *P* value at the top left of the graph represents overall significance calculated by Krusal-Wallis test. (**C**) The combined data of dbp43-specific kill are shown. Each symbol represents 1 mouse; horizontal bars indicate mean values. The *P* value at the top left of the graph represents overall significance calculated by Krusal-Wallis test.

the IgG1 isotype was not observed in LoxP-TAg mice with sporadic tumors, TAg recognition in the viral context apparently induced functionally different CD4$^+$ T cells. During subsequent HCC progression, anti-TAg IgG serum titers increased to dramatically high levels (Figure 2A). In order to directly assess the role of T cells during HCC development, CD4$^+$ and CD8$^+$ T cell–deficient LoxP-TAg mice were infected with Ad.Cre. The absence of both CD4$^+$ T cells and CD8$^+$ T cells substantially reduced the latency of virus-induced HCC in comparison with that in T cell competent–LoxP-TAg littermates (Figure 2C). Similarly, strongly accelerated HCC development was observed in combined Rag-2/IL-2 receptor γ chain–deficient LoxP-TAg mice, which lack T cells, B cells, and NK cells (Figure 2D). Because the immune deficiency also might have abolished antiadenoviral T cell responses and clearance of virus-infected cells, HCCs were induced by viral infection in villin-Cre (Vil-Cre) × LoxP-TAg double-transgenic mice. Due to constitutive stop cassette deletion and TAg activation in epithelial cells of the gastrointestinal tract, these mice had developed neonatal cytotoxic T lymphocyte (CTL) tolerance for TAg but were otherwise immune competent (32). Virus-induced HCC developed with similar reduced latency in Vil-Cre × LoxP-TAg mice as in T cell–deficient mice (Figure 2E). Collectively, the data indicate that virus-induced TAg activation in hepatocytes led to T cell immunity, which inhibited but did not prevent HCC development long term. Furthermore, TAg-specific T cells were mainly responsible for impairing HCC progression.

Virus-induced HCCs "sneak through" despite persistently functional CTLs. In LoxP-TAg mice with sporadic tumors, anti-TAg IgG antibodies predicted TAg-specific CTL tolerance (31). In contrast, in vivo CTL assays in Ad.Cre-infected LoxP-TAg mice revealed that functional CTLs directed against the immunodominant TAg pIV were induced as early as 2 weeks after virus infection (Figure 3, A and B). Remarkably, pIV-specific CTLs persisted in the presence of progressing TAg$^+$ HCC (Figure 3B). The strongest pIV-specific CTL

Table 1
LoxP-TAg mice with Ad.Cre-induced HCC reject s.c. transplanted TAg$^+$ tumor cells

Genotype	Time after Ad.Cre (wk)	Tumor take[A]	Time observed (wk)[B]
Rag2$^{-/-}$	–	3/3	[5, 6, 6][C]
Young Tg	–	0/4	30, 30, 30, 30[D]
Tg, sporadic	–	2/2	[5, 8][C]
Tg	4	2/13	10, 12, 18, 18, 18, 19, 19, 20, 22, 25, 29, [10, 11][C]
Tg	8	0/8	8, 8, 10, 10, 14, 14, 16, 20
Tg	24	0/3	8, 10, 12

1×10^6 TAg$^+$ 16.113 cells were injected s.c. into untreated 8- to 12-week-old Rag-2–deficient mice, LoxP-TAg mice (Young Tg), LoxP-TAg mice bearing large sporadic tumors (Tg, sporadic), and LoxP-TAg mice that had been injected with Ad.Cre when they were 8–12 weeks old (Tg). Tumor growth was followed using calliper measurement. [A]The number of mice with challenge tumor per mice in experiment is shown. Mice were observed until [B]they had to be sacrificed because of primary HCC or [C]challenge tumor grew to an average size of at least 6 mm in diameter (for these mice, time to growth of transplanted tumor cells is given in brackets). [D]Young LoxP-TAg mice observed for the indicated time were tumor free.

activity was detected in mice with large tumor burdens, suggesting that the progressing HCC upregulated CTL activity in the spleen (Figure 3B, white circles). CTLs specific for the adenovirus protein DNA-binding protein 43 (dbp43) were also induced upon Ad.Cre infection and were detectable by in vivo kill analysis throughout the experiment (Figure 3C).

As a more rigorous test for functional pIV-specific CTLs, HCC-bearing LoxP-TAg and — as controls — Rag-2–deficient mice, young LoxP-TAg mice, and old LoxP-TAg mice with sporadic tumors were challenged s.c. with the TAg-expressing tumor cell line 16.113 (Table 1). Whereas in Rag-2–deficient mice tumors grew, most LoxP-TAg mice infected with viruses 4, 8, and 24 weeks before (22 out of 24 mice) rejected the transplanted tumor cells, while the primary TAg$^+$ HCC progressed. In accordance with previous observations, LoxP-TAg mice with sporadic tumors did not reject 16.113 cells, whereas young LoxP-TAg mice rejected the transplanted tumor cells. Thus, TAg-specific CTLs, functionally activated upon virus-mediated TAg expression, were not systemically tolerized by the progressing HCC. Furthermore, the few TAg$^+$ cells that escaped elimination after viral infection "sneaked through" in the presence of functionally activated pIV-specific CTLs.

Virus-induced HCCs are regressors upon transplantation. Since HCCs progressed despite tumor immunity, we asked whether the HCCs were selected for low immunogenicity. Western blot analysis revealed that primary cell lines derived from HCCs of virus-infected LoxP-TAg mice expressed similar amounts of TAg when compared to the sporadic tumor line 16.113 and HCC cell lines that had been obtained from neonatal TAg-tolerant LoxP-TAg × Alb-Cre mice (Figure 4A). In order to determine the immunogenicity of TAg$^+$ HCC cell lines, B6 mice were immunized with cells of the respective HCC lines, and in vivo kill analysis was performed. A vigorous pIV-specific CTL response to all HCC cell lines was induced irrespective of whether they were obtained from virus-infected LoxP-TAg or TAg-tolerant LoxP-TAg × Alb-Cre mice (Figure 4B). The efficacy of TAg-specific CTL killing induced by the HCC lines was comparable to that induced by the sporadic regressor cell line 16.113. Importantly, all HCC lines used for in vivo kill analysis grew in immune-deficient *Rag2*$^{-/-}$ mice but were rejected when transplanted into immunocompetent B6 mice (Figure 4B). Therefore, no selection for low immunogenicity occurred in TAg-expressing HCC, despite the persistent presence of functional pIV-specific CTLs.

Virus-induced HCCs induce antigen-specific local tolerance. The previous experiments raised the question of how the HCCs, regressors upon transplantation, could progress in the presence of functional pIV-specific T cells. Histopathological examination of livers from nontreated and Ad.Cre-infected LoxP-TAg mice at different time points thereafter revealed moderate infiltration of the tumor nodules by CD3$^+$ T cells (Figure 5A). Quantitative analysis of CD3$^+$ T cell infiltration revealed significantly higher infiltration of small tumor nodules that developed 6–10 weeks after Ad.Cre infection in comparison with that of end-stage HCCs in mice 12–35 weeks after Ad.Cre infection. Peritumoral CD3$^+$ T cell infiltration in end-stage tumors was only slightly higher (statistically not significant) than intratumoral infiltration (Supplemental Figure 6). Whereas FoxP3$^+$ cells were not detected (Figure 5A), F4/80$^+$ cells, comprising macrophages and Kupffer cells, were equally distributed in the livers of naive and virus-infected mice (Figure 5A, weeks 0–4) but were decreased in cancerous tissue (Figure 5A, weeks 6–10 and 12–35). Solid tumors are supposed to create an immunosuppressive environment. We detected CD163$^+$ M2 macrophages, FAP$^+$ stromal cells, and CD11b$^+$/Gr-1$^+$ immature myeloid cells in end-stage HCC (Supplemental Figure 7). Therefore, these components potentially could contribute to local immune suppression. To analyze local T cell function in HCC, 16.113 cells, transduced to express luciferase (Fluc) and EGFP (16113^{gl}), were injected into the livers of virus-induced HCC-bearing LoxP-TAg mice, and mice were observed until they had to be sacrificed due to primary HCC burden. Histological analysis of liver sections revealed the growth of 16.113^{gl} tumors with the typical ductal appearance of this (gastrointestinal-derived) tumor, TAg-specific staining, and absence of the liver/HCC-specific marker HepPar1 in both HCC-bearing LoxP-TAg and *Rag2*$^{-/-}$ mice (Figure 5B). Age-matched tumor-free LoxP-TAg mice rejected 16.113^{gl} cells injected into the liver (data not shown). Because 16.113 cells were rejected in HCC-bearing mice at a s.c. injection site (Table 1), the data demonstrate local tolerance in HCC-bearing LoxP-TAg mice.

16.113 cells were transduced to express luciferase and EGFP (16113^{gl}) not only to visualize tumor growth but also to express foreign antigens in the tumor cells. This allowed us to ask whether tolerance in the tumor microenvironment was specific for TAg, the dominant transplantation rejection antigen in TAg-transformed tumors (8), or whether CTLs were suppressed independent of their specificity. First, 16113^{gl} cells were injected s.c. to analyze whether variants that lost the marker proteins (or the coexpressed selectable markers neomycin and hygromycin) could be selected in suitable hosts. In *Rag2*$^{-/-}$ mice, tumors grew and retained Fluc expression, as detected by BL imaging (Figure 5C). In LoxP-TAg × Alb-Cre mice, which are TAg tolerant but generate normal CTL responses to other antigens (31), Fluc (and EGFP; data not shown) signals became undetectable within 2 to 3 weeks (Figure 5, C and D), while TAg$^+$ tumors progressed after a short selection phase (Figure 5D). In young LoxP-TAg mice, 16113^{gl} tumors were rejected. Compatible with previous experiments, in old LoxP-TAg mice with sporadic tumors, which had developed TAg tolerance and CTL hyporesponsiveness to unrelated antigens (31), 16113^{gl}

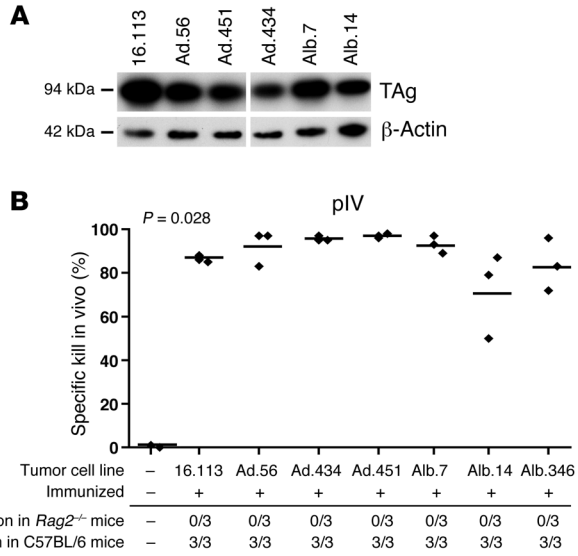

Figure 4

Transplanted Ad.Cre-induced HCCs from LoxP-TAg mice are as immunogenic as those from TAg-tolerant LoxP-TAg × Alb-Cre mice. (**A**) Similar TAg expression in HCC lines derived from Ad.Cre-treated LoxP-TAg mice and LoxP-TAg × Alb-Cre mice. Western blot analysis of TAg expression in primary HCC lines derived from Ad.Cre-treated LoxP-TAg mice (Ad.56, Ad.451, Ad.434) and LoxP-TAg × Alb-Cre mice (Alb.7, Alb.14). Sporadic TAg$^+$ tumor line 16.113 was used as a control. 20 μg protein was separated by SDS-PAGE gel, blotted onto nitrocellulose membrane, and incubated with anti-TAg antibodies. After autoradiography, the membrane was stripped and reprobed with anti–β-actin antibodies as loading control. The lanes were run on the same gel but were noncontiguous. (**B**) TAg$^+$ HCC lines induced pIV-specific CTLs. 1 × 10^6 cells of tumor lines 16.113 and HCC lines as indicated were injected s.c. into B6 mice, and 10 days later pIV-specific in vivo kill was assays were performed as in Figure 3. The percentage of specific killing of peptide-loaded cells is indicated. Each symbol represents 1 mouse; bars indicate mean values. The *P* value represents overall significance of the graph calculated by Krusal-Wallis test. In a separate experiment, 1 × 10^6 TAg$^+$ HCC cells and, as a control tumor line, 16.113 cells, were injected s.c. into untreated 8- to 12-week-old Rag-2–deficient and immunocompetent B6 mice. Tumor growth was followed using calliper measurement. Shown is the number of mice that rejected challenge tumor per mice in experiment. Mice were observed until challenge tumors grew up to an average size of at least 10 mm in diameter. Mice that rejected the transplanted tumor cells were observed for at least 90 days.

tumors grew progressively, while retaining the Fluc signal, albeit at reduced level (Figure 5, C and D). These data show that antigen loss variants can be selected but not in mice with nonvirus-induced sporadic cancer, leading to impaired CTL responses against unrelated antigens. Remarkably, if 16113^{gl} cells were injected intrahepatically (i.h.) into LoxP-TAg mice with virus-induced HCC, Fluc signals were lost within 2 to 3 weeks (Figure 5E and Supplemental Figure 8), and antigen loss variants progressed (Figure 5B). These data demonstrate that, in LoxP-TAg mice with virus-induced HCC, local tolerance is specific for the tumor transplantation rejection antigen TAg and that foreign antigens were still selected against in the tumor microenvironment.

Local tolerance is mediated by PD-1/PD-L1 dependent and independent mechanisms. pIV-specific CD8$^+$ T cells in livers and spleens of LoxP-TAg mice with virus-induced HCC were analyzed with K^b/IV tetramers. A high frequency of the CD8$^+$ T cells in the livers of HCC-bearing LoxP-TAg mice were pIV specific (14%–31% K^b/IV-tetramer$^+$ cells of the CD8$^+$ T cells) but not in age-matched nontreated LoxP-TAg mice (Figure 6A). The frequency of K^b/IV-tetramer$^+$ CD8$^+$ cells in the spleens of HCC-bearing LoxP-TAg mice was 5%–6%, whereas it was undetectable in the control mice. Importantly, programmed cell death protein-1 (PD-1) receptor was expressed on almost all K^b/IV-tetramer$^+$ CD8$^+$ T cells in the liver (Figure 6B). PD-1 expression was higher on liver compared with that on spleen pIV-specific CD8$^+$ T cells (Supplemental Figure 9). All virus-induced HCC cell lines investigated expressed the ligand PD-L1, whereas hepatocytes from noninfected LoxP-TAg mice did not (Figure 6C). In addition, immunohistochemical analysis of livers from HCC-bearing LoxP-TAg mice showed PD-L1 expression on TAg-positive carcinoma cells and TAg-negative stromal cells (Supplemental Figure 10). Notably, intrahepatic CD11c$^+$, CD68$^+$, and Gr-1$^+$ cells showed upregulation of PD-L1 when HCC-bearing LoxP-TAg mice 10–20 weeks after Ad.Cre infection were compared with untreated age-matched LoxP-TAg mice (Supplemental Figure 11). The sporadic tumor cell line 16.113 that grew in livers of HCC-bearing mice also expressed PD-L1 (Figure 6C).

Previous studies suggested that accessibility of T cells to the liver and lack of local inflammation prevented T cells from inducing autoimmunity and liver damage (33). If such a mechanism would be operative in our model, blockade of PD-1 should not be effective. To test this possibility, we blocked PD-1/PD-L1 interactions. LoxP-TAg mice with HCC 12 weeks after virus infection were treated with anti–PD-L1 antibodies for 2 weeks, revealing a significant delay in HCC progression when compared with mice that received isotype control antibodies (Figure 6D). The data are in agreement with data in HBV transgenic mice showing functional suppression of virus-specific CD8$^+$ T cells by PD-1/PD-L1 interaction (34). However, this study left open whether other mechanisms contributed to CD8$^+$ T cell suppression and whether PD-1$^+$CD8$^+$ T cells could suppress primary PD-L1$^+$ HCC in a permissive host. We also analyzed pIV-specific CD8$^+$ T cells in the liver for the presence of other inhibitory receptors involved in T cell exhaustion, namely Lag3, Tim-3, and CD160. We found that a high proportion of intrahepatic pIV-specific CD8$^+$ T cells expressed Lag3, CD160, and, occasionally, Tim-3 (Supplemental Figure 12). Next, we transferred spleen or CD8$^+$ T cells from LoxP-TAg mice with virus-induced HCC, which express PD-1 on almost all pIV-specific CD8$^+$ T cells (Figure 6B), into LoxP-TAg mice with virus-induced HCC after irradiation. Two weeks after treatment, mice with both spleen (Figure 6E) and CD8$^+$ T cell transfer (Figure 6F) and irradiation controls showed liver damage, as detected by increasing ALT and AST levels in the serum, likely due to irradiation (Supplemental Figure 13). Whereas in the irradiated control mice, ALT and AST levels further increased and mice rapidly succumbed to HCC, liver enzymes in immune cell–treated mice declined to slightly elevated levels in comparison with nontreated age-matched LoxP-TAg mice (Supplemental Figure 13). Spleen and CD8$^+$ T cell transfer substantially delayed HCC progression when compared with that in the irradiated control mice (Figure 6, E and F). Then, we repeated the experiment but treated LoxP-TAg mice 1, 7, and 19 weeks after virus infection. In mice treated 1 week and 19 weeks after viral infection the therapy was ineffective (Supplemental Figure 14, A and C). Probably, the few TAg$^+$ cells that survived clearance of most infected cells in the acute phase also escaped the transferred T cells. Nineteen weeks after viral infection, HCC was apparently too advanced for treatment. Treatment

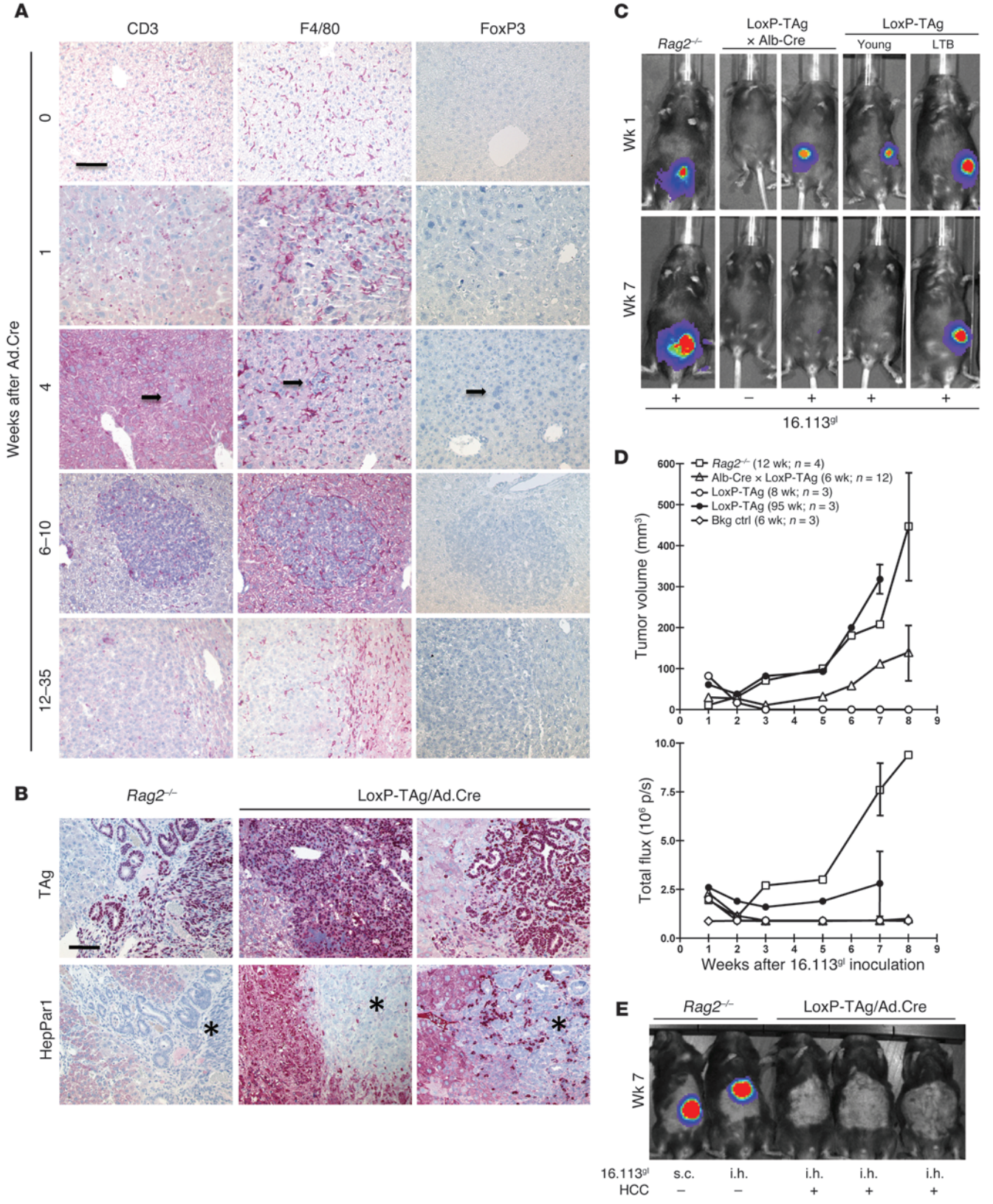
A
CD3
F4/80
FoxP3
Weeks after Ad.Cre
0
1
4
6–10
12–35
B
Rag2−/−
LoxP-TAg/Ad.Cre
TAg
HepPar1
C
Rag2−/−
LoxP-TAg × Alb-Cre
LoxP-TAg
Young
LTB
Wk 1
Wk 7
+ − + + +
16.113gl
D
Rag2−/− (12 wk; n = 4)
Alb-Cre × LoxP-TAg (6 wk; n = 12)
LoxP-TAg (8 wk; n = 3)
LoxP-TAg (95 wk; n = 3)
Bkg ctrl (6 wk; n = 3)
Tumor volume (mm3)
Total flux (10^6 p/s)
Weeks after 16.113gl inoculation
E
Rag2−/−
LoxP-TAg/Ad.Cre
Wk 7
16.113gl s.c. i.h. i.h. i.h. i.h.
HCC − − + + +

Figure 5
Ad.Cre-induced HCCs in LoxP-TAg mice cause antigen-specific local tolerance. (**A**) HCC tissues were stained for CD3, F4/80, and FoxP3 expression. Arrows indicate a small TAg$^+$ lesion (also depicted in Figure 1D). One representative out of three experiments per time point is shown. (**B**) 1×10^6 TAg$^+$ 16.113^{gl} cells were injected i.h. into *Rag2*$^{-/-}$ and HCC-bearing LoxP-TAg mice, and 7–12 weeks later liver tissues were stained for TAg and HepPar1. HepPar1-negative areas indicate 16.113 tumors (asterisks). Note that tumors grew in both groups of mice. Scale bar: 100 μm (**A** and **B**). (**C**) Selection of antigen-loss variants of 16.113^{gl} cells in LoxP-TAg × Alb-Cre but not *Rag2*$^{-/-}$ mice. LoxP-TAg × Alb-Cre (6 weeks), young LoxP-TAg (8 weeks), large tumor-bearing LoxP-TAg (95 weeks), and *Rag2*$^{-/-}$ mice (8–12 weeks) injected s.c. with 1×10^7 16113^{gl} cells were analyzed by BL imaging and tumor growth. Nontreated mice injected with luciferin served as controls (–; bkg ctrl). Images are representative for 2 experiments. (**D**) Tumor growth and Fluc signals of mice shown in **C**. Data shown are combined from 2 experiments; error bars represent SEM. Age and number of mice are shown in parenthesis. (**E**) Loss of BL signal of i.h. injected 16.113^{gl} cells in HCC-bearing LoxP-TAg mice, but not in *Rag2*$^{-/-}$ mice, 2–6 months after Ad.Cre infection, as detected by BL imaging. Representative *Rag2*$^{-/-}$ (s.c., $n = 2$; i.h., $n = 4$) and HCC-bearing mice (i.h., $n = 14$) 7 weeks after 16.113^{gl} cell injection are shown. See also Supplemental Figure 8.

7 weeks after viral infection (Supplemental Figure 14B) was similarly effective as that after 12 weeks (Figure 6, E and F). Together, both PD-1/PD-L1–dependent and –independent mechanisms appear to contribute to local tolerance. Furthermore, PD-1$^+$CD8$^+$ T cells have the potential to eliminate HCC in conditioned hosts.

Discussion

We established a model that recapitulates several features of virus-induced HCC in humans. A strong viral antigen, for which the mice were not tolerant at young age, was activated and recognized by T cells during viral infection of hepatocytes. The virus infection induced an antiviral response concomitant with a rapid and strong response against TAg, the cancer-driving oncogene, due to stop cassette deletion in the infected hepatocytes. T cell recognition resulted in hepatitis and clearance of the infected TAg$^+$ cells, at least the vast majority. Because adenoviruses do not replicate in mice, we ensured that the very few remaining TAg$^+$ hepatocytes escaped elimination and were not induced by virus spread. It remains enigmatic why these few TAg$^+$ hepatocytes survived, while neighboring infected TAg$^+$ cells were eliminated. They could have expressed less TAg during the effector CTL response (35), deleted the stop cassette when effector CTLs already went through the contraction phase (36), or reflected a subtype of hepatocytes that are resistant to elimination (37, 38). Strikingly, the few TAg$^+$ hepatocytes that sneaked through, despite functionally activated TAg-specific CTLs, were recognized at some point and upregulated systemic tumor immunity, at least at sites distant from the primary tumor, while progressing to lethal HCC. Sneaking through has been described previously in tumor transplantation models, in which low numbers of injected tumor cells remained unrecognized for too long by T cells (39). Sneaking through had not been demonstrated before in a primary tumor model in the presence of functionally activated CTLs.

Our data illustrate the fundamentally different immune response to sporadic and virus-induced tumors, directed against the same antigen in the same mouse model. If left untreated, LoxP-TAg mice develop in a stochastic manner sporadic tumors late in life after a long premalignant phase (8, 31). TAg recognition in mice with premalignant lesions, as detected by the generation of anti-TAg IgG antibodies, induced CTL tolerance, and no transient phase of functional activation was detected (31). In sharp contrast, if TAg was recognized by T cells during viral infection, anti-TAg antibodies were of partially different IgG subtype, indicating already the qualitatively different adaptive immune response. More importantly, in the viral context, CD4$^+$ and CD8$^+$ T cells were functionally activated and substantially delayed HCC progression. The response was primarily directed against TAg, because TAg-tolerant mice rapidly succumbed to HCC. In contrast to (nonvirus-induced) sporadic tumors, the virus-induced HCC needed to escape immune control. Immune escape did not involve systemic CTL tolerization or the apparent selection of low immunogenic variants. However, the observation that HCCs, progressors in the primary host with systemic tumor immunity, were regressors in transplantation experiments raises doubts about the ability of this assay to measure immune selective processes in the primary host.

There is ample evidence that solid tumors create an immune-suppressive microenvironment (40, 41). Therefore, it may not be surprising that transplanted TAg$^+$ tumor cells, which were rejected at a distant site, a phenomenon termed concomitant immunity (42), grew in the livers of HCC-bearing mice. Because most described immune-suppressive mechanisms, e.g., those mediated by indoleamine 2,3-dioxygenase, TGF-β1, FAP-expressing cells, M2 macrophages, or CD11b$^+$Gr1$^+$ cells (43–47), act nonspecifically, one would have expected that tumor-unrelated T cell responses were also suppressed within the suppressive tumor microenvironment. Remarkably, transplanted tumor cells were selected against expression of foreign antigen but not TAg in the livers of HCC-bearing mice, demonstrating local tolerance specifically for the rejection antigen of HCC. Tolerance required the presence of HCC, because young untreated LoxP-TAg mice rejected TAg$^+$ tumor cells injected into the liver. Our data contrast those obtained in a tumor transplantation model, suggesting that tumors are a privileged site for bacterial growth (48). Because of the rapid growth of the transplanted tumor, bacterial accumulation could be observed for only 6 days after intratumoral injection. Therefore, it is not clear whether an innate or adaptive immune response was impaired and whether the bacteria would have been eliminated at a later time point. This model is also difficult to compare to ours, because the bacteria, *Listeria monocytogenes*, reside inside macrophages and CD4$^+$ T cells are mainly responsible for protection.

The virus-induced HCC used at least 2 independent mechanisms of local tolerance, each of which was necessary for unimpaired progression. PD-1, expressed by almost all TAg-specific CD8$^+$ T cells in HCC-bearing mice, and PD-L1, expressed by the HCC, together with the observation that a brief treatment with anti–PD-L1 blocking antibodies substantially delayed HCC progression, reveal the first immune escape mechanism. We cannot exclude a contribution of PD-L1 expression by tumor stroma cells for T cell inhibition. This appears even likely, because various tumor stroma cell types expressed PD-L1 (49–52). PD-1 expression by CD8$^+$ T cells has been associated with cellular exhaustion in models of persistent viral infection (6, 53). Even though we cannot rule out some functional impairment of the TAg-specific PD-1$^+$CD8$^+$ T cells (5), they exhibited undiminished CTL activity in vivo, rejected TAg$^+$ tumor cells injected at a s.c. site and, importantly, inhibited autochthonous HCC progression upon transfer into sublethally irradiated mice. In fact, CTL activity was upregulated as HCC progressed and antigen amount was increased. Thus, while PD-1/PD-L1 interaction was clearly involved in local immune suppression, it was not sufficient to constrain HCC progression. We found additional inhibitory receptors, Lag3, CD160,

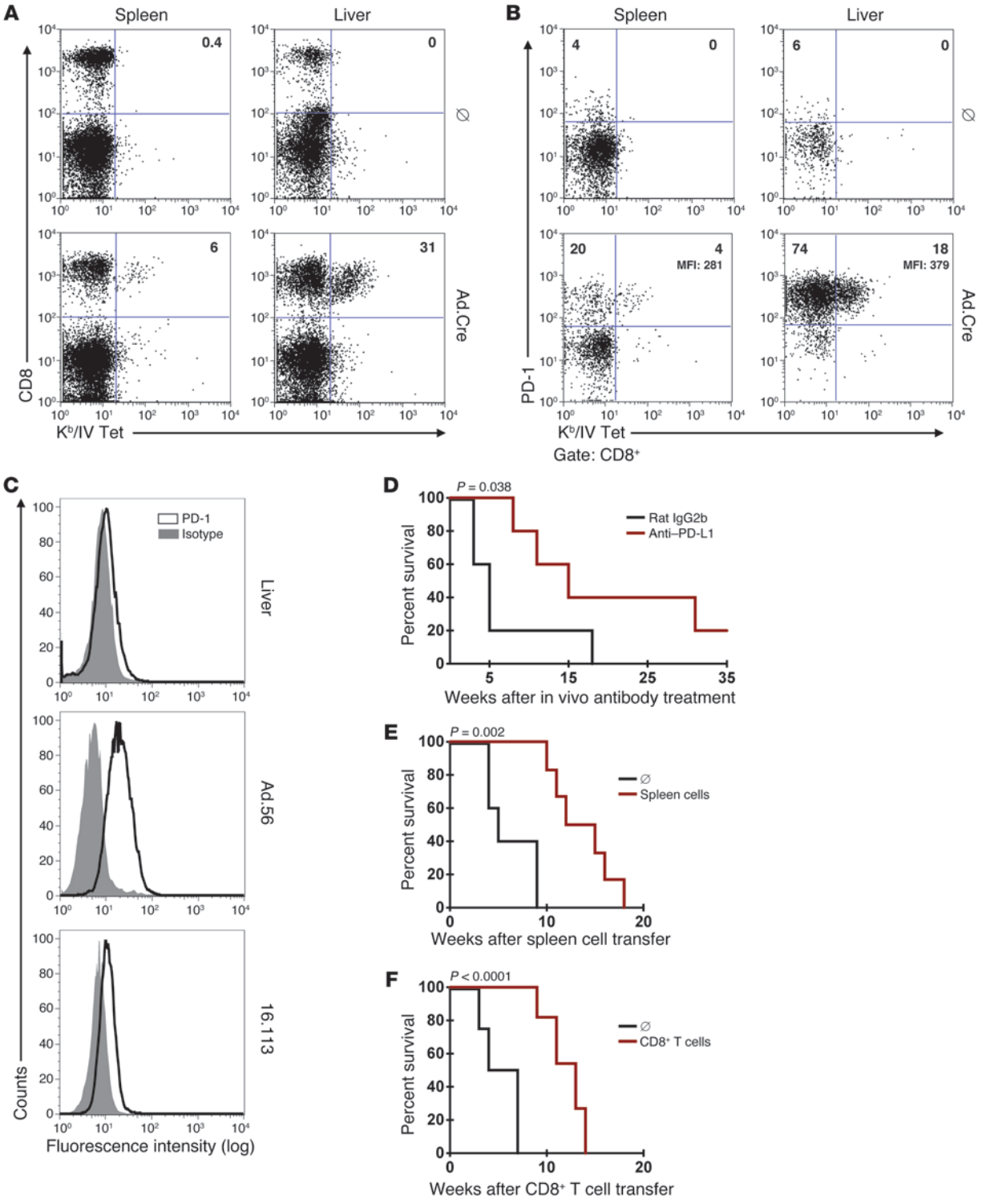
A
Spleen
Liver
0.4
0
6
31
∅
Ad.Cre
CD8
Kᵇ/IV Tet
B
Spleen
Liver
4
0
6
0
20
4
MFI: 281
74
18
MFI: 379
∅
Ad.Cre
PD-1
Kᵇ/IV Tet
Gate: CD8⁺
C
PD-1
Isotype
Liver
Ad.56
16.113
Counts
Fluorescence intensity (log)
D
P = 0.038
Rat IgG2b
Anti–PD-L1
Percent survival
Weeks after in vivo antibody treatment
E
P = 0.002
∅
Spleen cells
Percent survival
Weeks after spleen cell transfer
F
P < 0.0001
∅
CD8⁺ T cells
Percent survival
Weeks after CD8⁺ T cell transfer

Figure 6
Local tolerance is mediated by PD-1/PD-L1–dependent and –independent mechanisms. (**A**) Spleen and liver cells from nontreated and HCC-bearing LoxP-TAg mice 27 weeks after Ad.Cre infection were analyzed for CD8 expression and Kb/IV tetramer binding. Representative plots (n = 3; range from 14%–31% double-positive cells) are shown. (**B**) CD8$^+$ T cells as in **A** were analyzed for PD-1 expression and Kb/IV tetramer binding. Representative plots (n = 4; 7%–23% of Kb/IV tetramer$^+$ CD8$^+$ T cells expressed PD-1) are shown. (**C**) Hepatocytes from nontreated LoxP-TAg mice (liver), HCC line Ad.56, and 16.113 cells were stained with isotype control or anti–PD-L1 antibodies. Representative plots (n = 4) are shown. (**D**) HCC-bearing LoxP-TAg mice 12 weeks after Ad.Cre infection received anti–PD-L1 (red line, n = 5) or isotype control antibody (black line, n = 5) for 2 weeks, and survival was monitored. One of two experiments with comparable results is shown. (**E**) HCC-bearing LoxP-TAg mice 14 weeks after Ad.Cre injection (red line, n = 6) received irradiation (5 Gy) and 5 × 10^6 spleen cells from Ad.Cre-treated HCC-bearing LoxP-TAg mice (18 weeks after Ad.Cre injection) or were left untreated (black line, n = 5), and survival was monitored (see also Supplemental Figure 14B). (**F**) Irradiated HCC-bearing LoxP-TAg mice 16 weeks after Ad.Cre injection (red line, n = 11) were treated with 1 × 10^6 CD8$^+$ T cells obtained from mice as in **E** or left untreated (black line, n = 4), and survival was monitored.

and, occasionally, Tim-3, being expressed on pIV-specific T cells in the liver that could further contribute to T cell dysfunction in the liver (54–56). T cell accessibility of the HCC appeared to be a second mechanism impeding tumor immunosurveillance. It has been proposed that infiltration of adoptively transferred T cells in an autoimmune hepatitis model was facilitated by irradiation (57). Consistent with these data, the transfer of CD8$^+$ T cells from HCC-bearing mice, which contained TAg-specific CD8$^+$ T cells that basically all expressed PD-1$^+$, into irradiated HCC-bearing mice also substantially inhibited HCC progression. Virus-induced HCC in untreated mice contained fewer CD3$^+$ T cells in comparison with sporadic premalignant lesions of LoxP-TAg mice that had already developed CTL tolerance (31). Collectively, our data suggest a 2-stage immune evasive mechanism of HCC: T cells can only poorly infiltrate HCC, and the few infiltrating T cells are locally inhibited in their function. Blocking functional inhibition (through anti–PD-L1 antibodies) or allowing better T cell infiltration (through irradiation) overcomes local tolerance, albeit not long term.

While it has long been accepted that virus-associated cancers are under effective immunosurveillance (58), the mechanism of escape from immunosurveillance may be manifold and depend on the experimental or clinical situation. This is nicely illustrated by comparison of our model with a model published recently, in which lentiviruses were used to deliver neoantigens into cells, simultaneously deleting the p53 tumor suppressor and activating oncogenic Ras by Cre recombinase technology (59, 60). Depending on the site of tumor development, CTLs were either inefficiently activated (carcinomas in the lung) or efficiently activated CTLs selected antigen loss variants through epigenetic silencing (sarcomas in the muscle). The lentiviral and the adenoviral system presented here have common and distinct features, which together give important insight by which mechanism tumors escape under varying conditions. Both models have in common that the tumor antigen was expressed at the time of tumor initiation and was rapidly recognized by T cells during viral infection. On the other hand, both models likely differ by virus immunogenicity and infectivity, type of target antigen, mode of target antigen activation, and site of tumor development. One could have expected that tumor development in the liver, as a supposedly tolerogenic organ, rather than in the lung would have induced systemic tolerance, yet the opposite was the case. The high immunogenicity and the high infection rate of the adenovirus compared with that of the lentivirus may explain the different results. Thus, the adenovirus may act as stronger adjuvant to activate TAg-specific T cells compared with the lentivirus that helps the activation of the chosen model antigens SIY and ovalbumin (59, 60). Two reasons may explain the different mechanisms of immune escape in the HCC model (retention of the target antigen/high immunogenicity and local tolerance) versus the sarcoma model (loss of target antigen and selection for low immunogenicity). Sequences introduced into cells by viral infection may be silenced easier by epigenetic mechanisms than sequences introduced into the germline. More importantly, in the HCC model, the T cell response was directed against the cancer-driving oncogene, which cannot be easily selected against (61), while, in the sarcoma model, the T cell response was directed against surrogate antigens, which better reflect passenger mutations and can be easily selected against (60).

Because HCC progresses in a great proportion of patients with chronic HCV infection, despite the presence of HCV-specific CD8$^+$ T cells (15–17, 62), and the liver-infiltrating CD8$^+$ T cells in these patients expressed PD-1 (63), we think that our model encompassing both initial anti-virus immune response and HCC development bears high similarity to the human disease.

Methods

Mice. LoxP-TAg, Alb-Cre × LoxP-TAg, and Vil-Cre × LoxP-TAg transgenic mice were described previously (8, 31, 32). *Rag2*$^{-/-}$ mice (B6.129S6-Rag2^{tm1Fwa}) and *Rag2*$^{-/-}$*cg*$^{-/-}$ mice (C57BL/6J × C57BL/10SgSnAi)-[KO]γc-[KO]*Rag2*) were purchased from Taconics Farms; *Cd4*$^{-/-}$ mice (B6.129S2-*Cd4*^{tm1Mak}/J) and *Cd8*$^{-/-}$ mice (B6.129S2-*Cd8a*^{tm1Mak}/J) were purchased from The Jackson Laboratory; B6 mice were obtained from Charles River; and CD45.1 congenic mice were bred in our animal facilities.

Immunization/tumor cell transplantation. For TAg-specific immunization, mice were injected i.p. with 5 × 10^6 to 10 × 10^6 TAg$^+$ 16.113 tumor cells. Adenovirus-specific immunization was performed by i.v. injection of 1 × 10^9 PFUs of Ad.Cre. For tumor challenge experiments and analysis of TAg-specific CTL response, mice were injected s.c. with 1 × 10^6 cells of the indicated cell lines: 16.113 is a tumor cell line that developed spontaneously in the gastrointestinal tract of a LoxP-TAg mouse (8), HCC cell lines Ad.56/Ad.451/Ad.434 were obtained from LoxP-TAg mice 5–6 months after Ad.Cre administration, and HCC cell lines Alb.7/Alb.14/Alb.346 were isolated from 3-month-old LoxP-TAg × Alb-Cre mice (31). For analysis of local tolerance in the liver, 16.113 cells were retrovirally transduced with pLGSN and subsequently transfected with pCAG-Fluc generating cell line 16.113^{gl}. For selection of transduced and transfected clones neomycin and hygromycin resistance markers were used, respectively. 1 × 10^6 16.113^{gl} cells (bulk culture) expressing EGFP and Fluc were injected into the liver parenchyma, and growth of 16.113^{gl} cells was determined by histology of liver tissue sections. Tumor volume in mice injected s.c. with 1 × 10^7 16.113^{gl} cells into the flank was determined by caliper measurement of the tumor parameters (x,y,z) according to the formula (xyz)/2. Animals that rejected the challenge tumors were monitored for at least 60 days.

In vivo kill assays. CTL activity against the TAg-specific pIV (VVYDFLKL; ref. 8) was analyzed in vivo separately or simultaneously with the adenovirus dbp43 (FALSNAEDL; ref. 64). Single pIV-specific in vivo kill assay was performed as previously described (8). For simultaneous detection of CTL activity against pIV and dbp43, nonloaded (Ø)and pIV- and dbp43 peptide–loaded (1 μM each) CD45.1$^+$ congenic spleen cells (1 × 10^7

each) were labeled with CFSE in a final concentration of 0.75 μM ($CFSE^{hi}$), 0.075 μM ($CFSE^{int}$), or 0.0075 μM ($CFSE^{lo}$), respectively. A total of 3×10^7 mixed cells at a 1:1:1 ratio were injected i.v. into the indicated mice. 18 hours later, spleens of recipient mice were stained with APC-labeled anti-CD45.1 antibodies (A20, BD Pharmingen) to separate CFSE-labeled cells. The ratios among the 3 populations were determined by flow cytometry, and the specific cytolytic activity was calculated as follows: percentage of specific killing = (1 – [ratio of control mice/ratio of immunized] or 1 – [ratio of control mice/Ad.Cre-injected mice] × 100), where the ratio is the percentage of $CFSE^{lo}/CFSE^{hi}$ or $CFSE^{lo}/CFSE^{int}$.

ELISA. Serum samples from individual mice were collected. For detection of anti-TAg antibody, ELISA plates, coated with TAg protein, were used as described previously (8). Mouse TAg antibody (PAb 100; BD Pharmingen) was used as standard. TAg-specific IgG1, IgG2a, IgG2b, and IgG3 were determined in serum samples, obtained from individual mice. The mouse immunoglobulin screening/isotyping kit (Zymed Laboratories Inc.) was used according to the manufacturer's instructions.

Histology and immunohistochemistry. During autopsies of LoxP-TAg mice, whole organs or macroscopically detectable tumor tissues were embedded in paraffin. Serial sections (2–4 μm) were mounted on slides and stained with hematoxylin and eosin. For immunostaining, consecutive slides were subjected to a heat-induced epitope retrieval step before incubation with the following antibodies: mouse anti–SV40 large T, small t antigen (PAb 108; BD Pharmingen), Ki-67 (TEC-3, Dako), CD3 (N1580, Dako), FoxP3 (FJK-16s, eBioscience), F4/80 (BM8, eBioscience), CD163 (M-96, Santa Cruz Biotechnology), fibroblast activation protein (FAP; Abcam), and HepPar1 (OCH1E5.2.10, Dako). For detection, the Streptavidin-AP Kit (K5005, Dako) alone or biotinylated donkey anti-rat (Dianova) or rabbit anti-rat (Dako) secondary antibodies were used followed by the Streptavidin-AP Kit or the EnVision Peroxidase Kit (K 4010, Dako). Alkaline phosphatase (AP) and peroxidase were developed by Fast Red as chromogen or diaminobenzidine chromogenic substrates, respectively. For double immunofluorescence staining, 5-μm cryosections were incubated first with FITC-labeled mouse anti–SV40 large T, small t antigen (PAb 108; BD Pharmingen) antibody. After washing 3 times in PBS, sections were incubated with anti-mouse PD-L1 (10F.9G2, BioLegend). After another washing step, sections were stained with Alexa Fluor 594–labeled donkey anti-rat antibody. Nuclei were counterstained using VECTASHIELD Hard+Set Mounting Medium with DAPI (Vector Laboratories). Images were acquired using a fluorescence microscope (AxioImager) equipped with a CCD camera (AxioCam MRm) and processed with ApoTome and ZEN software (Carl Zeiss MicroImaging Inc.).

Flow cytometry. Single cell suspensions of spleen cells were stained with PE-labeled K^b/pIV tetramers (Beckman Coulter), PerCP-labeled rat anti-mouse CD8a antibody (53-6.7; BD Pharmingen), APC-labeled hamster anti-mouse CD3a antibody (145-2C11; BD Pharmingen), APC-labeled hamster anti-mouse CD279 antibody (J43; BD Pharmingen), PerCP-eFluor 710-labeled anti-mouse CD223 (Lag3, C9B7W; eBioscience), Alexa Fluor 647–labeled anti-mouse Tim-3 (B8.2C12, BioLegend), and eFluor 660–labeled anti-mouse CD160 (CNX46-3; eBioscience). For analysis of hepatic lymphocytes and hepatocytes, livers were perfused with PBS, collagenase digested (1 mg/ml, 4 hours, 37°C), washed twice, and subsequently incubated with the antibody indicated above or PE-conjugated rabbit anti-mouse CD274 (MIH5; BD Pharmingen) and isotype-matched control antibody.

In vivo MRI. MRI experiments were performed with a 1.5-T clinical MRI instrument (Magnetom Symphony Maestro Class, Siemens), with either a CP-Breast Array or a Flex Loop Small surface coil (Siemens) as previously described (31).

Detection of liver enzymes. The transaminases ALT and AST were used as indicators for liver damage. Serum samples, mixed with Heparin, were analyzed (Laboklin).

BL imaging. Mice were injected i.p. with 3 mg D-luciferin (Biosynth) dissolved in PBS (30 mg/ml). 10 minutes later, mice were anesthetized with isoflurane, and BL image acquisition was performed using an exposure time of 180 seconds. BL imaging data were analyzed with the Living Image software (Caliper Life Science). For detection of adenovirus tropism, an adenovirus expressing the firefly luciferase under the control of the CMV promoter (Ad. Luc), provided by M. Zenke (Institute for Biomedical Engineering, Cell Biology, Aachen University Medical School, RWTH Aachen, Germany), was used.

Western blot analysis. Proteins were quantified with the Bio-Rad protein assay. 40 μg protein extract was loaded onto a NuPage Tris-acetate 3%–8% SDS-PAGE gel (Invitrogen) and blotted on a polyvinylidene fluoride membrane (Amersham Biosciences) using the XCell II blot module (Invitrogen). After blocking with 5% dried skim milk, the blot was incubated with anti-TAg IgG2a antibody (Ab-2, Calbiochem), washed with PBS containing 0.5% Tween, and subsequently incubated with HRP-labeled anti-mouse IgG2a antibody (BD Biosciences). Visualization was performed using the ECL Detection Kit (Amersham Biosciences) according to the manufacturer's instructions and the LUMI-F1 Imaging Workstation (Roche). To confirm loading of equal amounts of protein, the blot was reprobed with anti–β-actin antibody (Abcam), followed by HRP-labeled goat anti-rabbit-IgG (BD Bioscience), and detected as described above.

Primary tumor induction. For HCC induction, LoxP-TAg mice (8) were infected with 1×10^9 PFUs of Cre recombinase–expressing adenoviruses (Ad.Cre) by tail vein injection (i.v.).

PD-L1 mAb treatment. For in vivo antibody blockade, 200 μg rat anti-mouse PD-L1 (10F.9G2; Bio X Cell) and rat IgG2b isotype control (LTF-2; Bio X Cell) were injected i.p. into the indicated mice every third day for 2 weeks as described previously (7), and HCC development was monitored.

Adoptive immune cell transfer. For adoptive cell transfer, splenic $CD8^+$ T cells were purified by use of the $CD8\alpha^+$ T Cell Isolation Kit II (Miltenyi Biotec). 1×10^6 purified $CD8^+$ T cells (80%–95% purity) were injected i.v. into irradiated (5 Gy) HCC-bearing LoxP-TAg mice. For spleen cell transfer, single cell suspensions were prepared, and 5×10^6 cells were transferred i.v.

Statistics. Statistical analyses were performed using SPSS and Prism (GraphPad) Software. The overall significance of each graph was calculated with the Kruskal-Wallis test. Comparisons of 2 groups were done by Mann-Whitney *U* test. Survival curves were compared by Gehan-Breslow-Wilcoxon test. *P* values of less than 0.05 were regarded as statistically significant.

Study approval. Animal experiments were performed according to and with approval of Landesamt für Gesundheit und Soziales, Berlin, Germany.

Acknowledgments

We thank K. Borgwald, S. Horn, K. Retzlaff, D. Barthel, S. Spieckermann, M. Roesch, A. Gaertner, and C. Westen for technical assistance. This work was supported by grants from the Deutsche Forschungsgemeinschaft (TR36, TR54, and SFB633), the "Alliance" program of the HGF (HA-202), and the clinical cooperation program of the Max Delbrück Center for Molecular Medicine Berlin (to G. Willimsky and J. Gellermann).

Received for publication May 10, 2012, and accepted in revised form December 6, 2012.

Address correspondence to: Thomas Blankenstein, Max Delbrück Center for Molecular Medicine, Robert-Rössle Str. 10, 13092 Berlin, Germany. Phone: 49.30.9406.2816; Fax: 49.30.9406.2453; E-mail: tblanke@mdc-berlin.de. Or to: Gerald Willimsky, Institute of Immunology, Charité Campus Berlin Buch, Lindenberger Weg 80, 13125 Berlin, Germany. Phone: 49.30.450.513607; Fax: 49.30.450.7513607; E-mail: gerald.willimsky@charite.de.

1. Blankenstein T. Do autochthonous tumors interfere with effector T cell responses? *Semin Cancer Biol*. 2007;17(4):267–274.
2. Klein G, Klein E. Rejectability of virus-induced tumors and nonrejectability of spontaneous tumors: a lesson in contrasts. *Transplant Proc*. 1977; 9(1):1095–1104.
3. Bowen DG, Zen M, Holz L, Davis T, McCaughan GW, Bertolino P. The site of primary T cell activation is a determinant of the balance between intrahepatic tolerance and immunity. *J Clin Invest*. 2004; 114(5):701–712.
4. Gruener NH, et al. Sustained dysfunction of antiviral CD8+ T lymphocytes after infection with hepatitis C virus. *J Virol*. 2001;75(12):5550–5558.
5. Lukens JR, Dolina JS, Kim TS, Tacke RS, Hahn YS. Liver is able to activate naive CD8+ T cells with dysfunctional anti-viral activity in the murine system. *PLoS One*. 2009;4(10):e7619.
6. Wherry EJ. T cell exhaustion. *Nat Immunol*. 2011; 12(6):492–499.
7. Barber DL, et al. Restoring function in exhausted CD8 T cells during chronic viral infection. *Nature*. 2006;439(7077):682–687.
8. Willimsky G, Blankenstein T. Sporadic immunogenic tumours avoid destruction by inducing T-cell tolerance. *Nature*. 2005;437(7055):141–146.
9. Kantzanou M, et al. Viral escape and T cell exhaustion in hepatitis C virus infection analysed using class I peptide tetramers. *Immunol Lett*. 2003;85(2):165–171.
10. Crispe IN. Hepatic T cells and liver tolerance. *Nat Rev Immunol*. 2003;3(1):51–62.
11. Lechner F, et al. Analysis of successful immune responses in persons infected with hepatitis C virus. *J Exp Med*. 2000;191(9):1499–1512.
12. Thimme R, Oldach D, Chang KM, Steiger C, Ray SC, Chisari FV. Determinants of viral clearance and persistence during acute hepatitis C virus infection. *J Exp Med*. 2001;194(10):1395–1406.
13. Grabowska AM, et al. Direct ex vivo comparison of the breadth and specificity of the T cells in the liver and peripheral blood of patients with chronic HCV infection. *Eur J Immunol*. 2001;31(8):2388–2394.
14. Lucas M, et al. Pervasive influence of hepatitis C virus on the phenotype of antiviral CD8+ T cells. *J Immunol*. 2004;172(3):1744–1753.
15. Wong DK, et al. Detection of diverse hepatitis C virus (HCV)-specific cytotoxic T lymphocytes in peripheral blood of infected persons by screening for responses to all translated proteins of HCV. *J Virol*. 2001;75(3):1229–1235.
16. Neveu B, et al. Selection of high-avidity CD8 T cells correlates with control of hepatitis C virus infection. *Hepatology*. 2008;48(3):713–722.
17. Barnes E, Ward SM, Kasprowicz VO, Dusheiko G, Klenerman P, Lucas M. Ultra-sensitive class I tetramer analysis reveals previously undetectable populations of antiviral CD8+ T cells. *Eur J Immunol*. 2004;34(6):1570–1577.
18. Spangenberg HC, et al. Intrahepatic CD8+ T-cell failure during chronic hepatitis C virus infection. *Hepatology*. 2005;42(4):828–837.
19. Grakoui A, et al. HCV persistence and immune evasion in the absence of memory T cell help. *Science*. 2003;302(5645):659–662.
20. Thomson M, et al. The clearance of hepatitis C virus infection in chimpanzees may not necessarily correlate with the appearance of acquired immunity. *J Virol*. 2003;77(2):862–870.
21. Bissig KD, et al. Human liver chimeric mice provide a model for hepatitis B and C virus infection and treatment. *J Clin Invest*. 2010;120(3):924–930.
22. Dorner M, et al. A genetically humanized mouse model for hepatitis C virus infection. *Nature*. 2011; 474(7350):208–211.
23. Jo J, Lohmann V, Bartenschlager R, Thimme R. Experimental models to study the immunobiology of hepatitis C virus. *J Gen Virol*. 2011;92(pt 3):477–493.
24. Kamegaya Y, et al. Hepatitis C virus acts as a tumor accelerator by blocking apoptosis in a mouse model of hepatocarcinogenesis. *Hepatology*. 2005; 41(3):660–667.
25. McGivern DR, Lemon SM. Virus-specific mechanisms of carcinogenesis in hepatitis C virus associated liver cancer. *Oncogene*. 2011;30(17):1969–1983.
26. Wakita T, et al. Possible role of cytotoxic T cells in acute liver injury in hepatitis C virus cDNA transgenic mice mediated by Cre/loxP system. *J Med Virol*. 2000;62(3):308–317.
27. Ernst E, et al. Generation of inducible hepatitis C virus transgenic mouse lines. *J Med Virol*. 2007; 79(8):1103–1112.
28. Takaku S, et al. Induction of hepatic injury by hepatitis C virus-specific CD8+ murine cytotoxic T lymphocytes in transgenic mice expressing the viral structural genes. *Biochem Biophys Res Commun*. 2003; 301(2):330–337.
29. Isogawa M, Furuichi Y, Chisari FV. Oscillating CD8(+) T cell effector functions after antigen recognition in the liver. *Immunity*. 2005;23(1):53–63.
30. Nakamoto Y, Guidotti LG, Kuhlen CV, Fowler P, Chisari FV. Immune pathogenesis of hepatocellular carcinoma. *J Exp Med*. 1998;188(2):341–350.
31. Willimsky G, et al. Immunogenicity of premalignant lesions is the primary cause of general cytotoxic T lymphocyte unresponsiveness. *J Exp Med*. 2008; 205(7):1687–1700.
32. Czéh M, et al. The immune response to sporadic colorectal cancer in a novel mouse model. *Oncogene*. 2010;29(50):6591–6602.
33. Limmer A, et al. Failure to induce organ-specific autoimmunity by breaking of tolerance: importance of the microenvironment. *Eur J Immunol*. 1998; 28(8):2395–2406.
34. Maier H, Isogawa M, Freeman GJ, Chisari FV. PD-1:PD-L1 interactions contribute to the functional suppression of virus-specific CD8+ T lymphocytes in the liver. *J Immunol*. 2007;178(5):2714–2720.
35. Wadsworth SC, Zhou H, Smith AE, Kaplan JM. Adenovirus vector-infected cells can escape adenovirus antigen-specific cytotoxic T-lymphocyte killing in vivo. *J Virol*. 1997;71(7):5189–5196.
36. Yang TC, Dayball K, Wan YH, Bramson J. Detailed analysis of the CD8+ T-cell response following adenovirus vaccination. *J Virol*. 2003; 77(24):13407–13411.
37. Kafrouni MI, Brown GR, Thiele DL. Virally infected hepatocytes are resistant to perforin-dependent CTL effector mechanisms. *J Immunol*. 2001; 167(3):1566–1574.
38. Kafrouni MI, Brown GR, Thiele DL. The role of TNF-TNFR2 interactions in generation of CTL responses and clearance of hepatic adenovirus infection. *J Leukoc Biol*. 2003;74(4):564–571.
39. Old LJ, Boyse EA, Clarke DA, Carswell EA. Antigenic properties of chemically-induced tumors. *Ann NY Acad Sci*. 1962;101:80–106.
40. Ganss R, Hanahan D. Tumor microenvironment can restrict the effectiveness of activated antitumor lymphocytes. *Cancer Res*. 1998;58(20):4673–4681.
41. Zou W. Immunosuppressive networks in the tumour environment and their therapeutic relevance. *Nat Rev Cancer*. 2005;5(4):263–274.
42. Gorelik E. Concomitant tumor immunity and the resistance to a second tumor challenge. *Adv Cancer Res*. 1983;39:71–120.
43. Uyttenhove C, et al. Evidence for a tumoral immune resistance mechanism based on tryptophan degradation by indoleamine 2,3-dioxygenase. *Nat Med*. 2003;9(10):1269–1274.
44. Flavell RA, Sanjabi S, Wrzesinski SH, Licona-Limón P. The polarization of immune cells in the tumour environment by TGFbeta. *Nat Rev Immunol*. 2010; 10(8):554–567.
45. Kraman M, et al. Suppression of antitumor immunity by stromal cells expressing fibroblast activation protein-alpha. *Science*. 2010;330(6005):827–830.
46. Sica A, Mantovani A. Macrophage plasticity and polarization: in vivo veritas. *J Clin Invest*. 2012; 122(3):787–795.
47. Gabrilovich DI, Nagaraj S. Myeloid-derived suppressor cells as regulators of the immune system. *Nat Rev Immunol*. 2009;9(3):162–174.
48. Spitalny GL, North RJ. Subversion of host defense mechanisms by malignant tumors: an established tumor as a privileged site for bacterial growth. *J Exp Med*. 1977;145(5):1264–1277.
49. Kuang DM, et al. Activated monocytes in peritumoral stroma of hepatocellular carcinoma foster immune privilege and disease progression through PD-L1. *J Exp Med*. 2009;206(6):1327–1337.
50. Curiel TJ, et al. Blockade of B7-H1 improves myeloid dendritic cell-mediated antitumor immunity. *Nat Med*. 2003;9(5):562–567.
51. Wu K, Kryczek I, Chen L, Zou W, Welling TH. Kupffer cell suppression of CD8+ T cells in human hepatocellular carcinoma is mediated by B7-H1/programmed death-1 interactions. *Cancer Res*. 2009; 69(20):8067–8075.
52. Scarlett UK, et al. Ovarian cancer progression is controlled by phenotypic changes in dendritic cells. *J Exp Med*. 2012;209(3):495–506.
53. Pardoll DM. The blockade of immune checkpoints in cancer immunotherapy. *Nat Rev Cancer*. 2012;12(4):252–264.
54. Blackburn SD, et al. Coregulation of CD8+ T cell exhaustion by multiple inhibitory receptors during chronic viral infection. *Nat Immunol*. 2009; 10(1):29–37.
55. Li H, et al. Tim-3/galectin-9 signaling pathway mediates T cell dysfunction and predicts poor prognosis in patients with HBV-associated hepatocellular carcinoma. *Hepatology*. 2012;56(4):1342–1351.
56. Mackay LK, et al. Maintenance of T cell function in the face of chronic antigen stimulation and repeated reactivation for a latent virus infection. *J Immunol*. 2012;188(5):2173–2178.
57. Ganss R, Limmer A, Sacher T, Arnold B, Hämmerling GJ. Autoaggression and tumor rejection: it takes more than self-specific T-cell activation. *Immunol Rev*. 1999;169:263–272.
58. Klein G, Klein E. Immune surveillance against virus-induced tumors and nonrejectability of spontaneous tumors: contrasting consequences of host versus tumor evolution. *Proc Natl Acad Sci U S A*. 1977;74(5):2121–2125.
59. DuPage M, et al. Endogenous T cell responses to antigens expressed in lung adenocarcinomas delay malignant tumor progression. *Cancer Cell*. 2011; 19(1):72–85.
60. DuPage M, Mazumdar C, Schmidt LM, Cheung AF, Jacks T. Expression of tumour-specific antigens underlies cancer immunoediting. *Nature*. 2012;482(7385):405–409.
61. Anders K, et al. Oncogene-targeting T cells reject large tumors while oncogene inactivation selects escape variants in mouse models of cancer. *Cancer Cell*. 2011;20(6):755–767.
62. Lauer GM, et al. Comprehensive analysis of CD8(+)-T-cell responses against hepatitis C virus reveals multiple unpredicted specificities. *J Virol*. 2002; 76(12):6104–6113.
63. Radziewicz H, et al. Liver-infiltrating lymphocytes in chronic human hepatitis C virus infection display an exhausted phenotype with high levels of PD-1 and low levels of CD127 expression. *J Virol*. 2007; 81(6):2545–2553.
64. McKelvey T, Tang A, Bett AJ, Casimiro DR, Chastain M. T-cell response to adenovirus hexon and DNA-binding protein in mice. *Gene Ther*. 2004; 11(9):791–796.